Accepted version: Chemistry and Physics of Lipids 239C (2021) 105117
Received 24 April 2021, Revised 3 July 2021, Accepted 9 July 2021, Available online 12 July 2021.

Lipid monolayer spontaneous curvatures: a collection of published values

Marcus K. Dymond[*1]

[1] Chemistry Research and Enterprise Group, School of Pharmacy and Biomolecular Sciences, Huxley Building, University of Brighton, BN2 4GL.

[*] Author for correspondence; M.Dymond@brighton.ac.uk

Abstract

Lipid monolayer spontaneous curvatures (or lipid intrinsic curvatures) are one of several material properties of lipids that enable the stored curvature elastic energy in a lipid aggregate to be determined. Stored curvature elastic energy is important since it can modulate the function of membrane proteins and plays a role in the regulatory pathways of phospholipid homeostasis. Due to the large number of different lipid molecules that might theoretically exist in nature, very few lipid spontaneous curvatures have been determined. Herein the values of lipid spontaneous curvatures that exist in the literature are collected, alongside key experimental details. Where possible, trends in the data are discussed and finally, obvious gaps in the knowledge are signposted.

Keywords: Lipid monolayer spontaneous curvature; lipid intrinsic curvature; membrane curvature; elastic theory of membranes; intrinsic curvature hypothesis

Accepted version: Chemistry and Physics of Lipids 239C (2021) 105117
Received 24 April 2021, Revised 3 July 2021, Accepted 9 July 2021, Available online 12 July 2021.

1.0 Introduction

The elastic theory of lipid membranes was developed by Helfrich [1] to describe how the free energy of lipid bilayers changes in response to the geometry they are confined within. Since its inception the elastic theory of membranes has enabled quantitative models of cell membrane-protein interactions to be developed [2,3], ultimately giving rise to the intrinsic curvature hypothesis i.e. that cells regulate the stored elastic energy of their bilayer membranes [4,5]. A key concept of the theory introduced by Helfrich is the idea of bilayer spontaneous curvature, which is typically determined using tether-pulling experiments [6]. Bilayer spontaneous curvatures can, as shown in giant unilamellar vesicles, vary with osmotic pressure induced by sugar molecules [7], or be controlled by membrane binding proteins [8]. However, because lipid bilayers comprise of two fused monolayers back-to-back, some of the properties of lipid bilayers can be modelled by considering the properties of the individual monolayer leaflets.

The lipid monolayer spontaneous curvature or lipid intrinsic curvature (c_0) is an important material parameter of lipids that enables curvature elastic energy in lipid monolayers to be quantified. Stored elastic energy arises in monolayers when lipids with a preference for one curvature are confined to a different curvature, known as curvature frustration. The curvature frustration concept is particularly relevant to cellular studies since many lipids found naturally within cell membranes do not readily form bilayers, but rather, preferentially form tightly curved structures, like the inverse hexagonal (H_{II}) structure [9]. Developing quantitative models of biological membranes, which take account of stored curvature elastic energy and its contribution to the regulation of membrane protein activity, via modification of membrane lipid composition [10], requires knowledge of the c_0 values of lipids, in addition to other elastic constants. Unfortunately, the time-consuming nature of determining c_0, coupled with the many thousands of different individual lipids, means that comparatively few values of c_0 have been reported. Herein those published c_0 values are collected and trends detailing the dependence of c_0 on ionic strength and temperature are briefly discussed. Prior to this, and for those new to the field, a brief overview of key elements of the elastic theory of membranes is provided, key texts detailing techniques to accurately measure c_0 are signposted, and examples of biological studies where c_0 values are vital to develop quantitative models are presented.

1.1 Curvature elastic energy in lipid aggregates

Curvature elastic energy in monolayers can be quantified by the Helfrich Hamiltonian, Equation 1, see Deserno [11] for a detailed review, where the elastic free energy (ΔG_c) of bending a monolayer of surface area A is

$$\Delta G_c = \tfrac{1}{2}\,\kappa_M A(c_1 + c_2 - c_0)^2 + \kappa_G A c_1 c_2 \qquad \text{Eq. 1}$$

such that, c_1 (=1/R_1) and c_2 (=1/R_2) are the principal curvatures of the interface (monolayers that curve toward water are defined as having negative curvature), κ_M is the monolayer bending rigidity and κ_G is the Gaussian curvature modulus. A fairly extensive review of the elastic constants κ_M and κ_G for individual lipids can be found in the literature [12]. c_0 is defined as 1/ R_0, i.e., the radius of curvature formed by an unstressed lipid aggregate. As noted [11], a degree of caution needs to be applied due to different conventions describing c_0 values, which is not always made clear in individual studies, since $c_0 = 2H_0$, where H_0 is the mean spontaneous curvature [13].

Accepted version: Chemistry and Physics of Lipids 239C (2021) 105117
Received 24 April 2021, Revised 3 July 2021, Accepted 9 July 2021, Available online 12 July 2021.

Determinations of R_0 are made using small angle X-ray diffraction, see Kozlov for detailed method [13], utilising inverse hexagonal lipid mesophases. Measurements on H_{II} phases have the distinct advantage that H_{II} phases are often stable in excess water. Since the lattice parameter (d_{hex}) of the inverse hexagonal phase stabilises above the limit of hydration, it was initially considered that this limit reflected the lipid spontaneous curvature. Later, however, studies of H_{II} phases under dual solvent stress [14] showed that the partitioning of hydrophobic solvents like dodecane into the interior of the H_{II} phase relieved packing stresses, allowing lipids to reveal an underlying propensity towards curved aggregates, now interpreted as c_0 [15]. DOPC is a classic example of this; in the absence of hydrocarbon, it forms a lamellar phase and in the presence of hydrocarbons it forms a H_{II} phase [16]. The position of the plane of measurement of R_0 is a critical definition, which involves choosing a dividing surface along the length of the lipid molecule. Measurements of c_0 have been made at the pivotal plane (R_p) (i.e. the plane where area per lipid does not change on monolayer bending), since this dividing surface was historically easier to identify than the neutral plane (R_n). However, the advantage of measuring c_0 values at the neutral plane arises because the elastic moduli of stretching and bending are independent at this dividing surface. As a result, changes in the free energy for deforming a lipid monolayer only require expressions with terms that relate to the pure bending and pure stretching deformations. In contrast at all other dividing surfaces a further term describing mixed deformation (i.e. concurrent stretching and bending) is required, hence measurements at the neutral surface simplify free energy calculations, particularly when tightly curved monolayers are considered [17].

Aided by electron density reconstructions of the H_{II} phase, which allow R_p to be determined, an increasing number of studies have emerged where c_0 is determined at the neutral plane [18–20]. This is enabled by using the relationship $R_0 = R_n = R_p + d_{H1}$, where d_{H1} is found to be *circa* 0.44 ± 0.05 nm for DOPE [18]. It is also worth noting that a number of studies rely on estimates of the position of the pivotal or neutral planes, which are taken from related lipid systems, to calculate c_0 [21–23]. Figure 1 shows the structure of the H_{II} phase and identifies the pivotal and neutral planes.

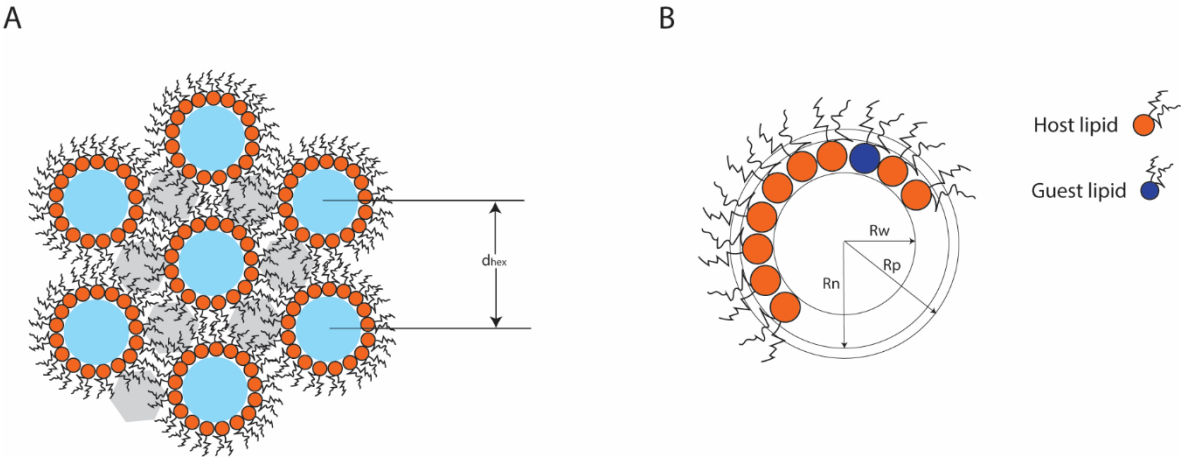

Figure 1. The structure of the inverse hexagonal phase and its relationship to measuring lipid monolayer spontaneous curvatures. Figure 1A shows the structure of the H_{II} phase, water occupies blue areas, grey shading indicates interstitial sites in relation to the hexagonal lattice parameter (d_{hex}). Figure 1B shows the structure of an individual lipid-lined water channel for a mixture of host and guest lipids. The radius of the water cylinder (R_w), radius of the pivotal plane (R_p) and radius of the neutral plane (R_n) are indicated.

Accepted version: Chemistry and Physics of Lipids 239C (2021) 105117
Received 24 April 2021, Revised 3 July 2021, Accepted 9 July 2021, Available online 12 July 2021.

Work on lipid mixtures suggests that the principles of linear additivity and ideal mixing can be applied to enable the spontaneous curvature of the lipid mixture (c_{0mix}) to be calculated from its components [24], as shown in Equation 2.

$$c_{0mix} = A_{MF}c_{0A} + B_{MF}c_{0B} + C_{MF}c_{0C} \ldots \text{etc.} \qquad \text{Eq. 2}$$

where A, B and C are individual lipid species and the subscripts $_{MF}$ and c_0 denote the mole fraction and c_0 values of each individual lipid component. It should be noted that Equation 2 is an *ad hoc* assumption and under certain circumstances, such as when there is a significant mismatch in lipid chain length, it does not hold valid, as shown by molecular dynamics simulations of lipid mixtures containing cholesterol or sphingomyelin [25].

The concept of ideal linear mixing enables the c_0 values of a range of other lipids to be calculated, most usefully lipids that don't form H_{II} phases [18]. This is the origin of the so-called host-guest technique for determining lipid monolayer spontaneous curvatures, shown in Figure 1B. Host lipids are lipids that form H_{II} phases, frequently DOPE, guest lipids are introduced at defined mole fractions, c_{0mix} is measured and the c_0 of the guest lipid is calculated using Eq. 2. Underpinning the calculation of c_0 in the literature are a couple of common assumptions. The first is that ideal linear mixing occurs, which is seemingly valid for low mole fractions of guest lipids. This, of course, means that all c_0 values determined by the host-guest method are subject to the assumption that Eq. 2 holds true. Where evidence of lateral phase separation exists; the assumption that ideal linear mixing occurs within the domains is used, if the lipid composition of these domains is known then the elastic properties of the mixture can be determined [18]. Secondly, many studies rely on the relatively low variation observed for $\bar{\kappa}_M$ values for different lipids and hence assume that $\bar{\kappa}_M$ is constant for the lipid mixture under study. Some c_0 calculations assume that c_0 is not dependent on temperature over the range studied. In general, such assumptions are well founded and clearly identified in the different studies. Inevitably, however, the limits of using them are revealed by systematic studies, suggesting caution needs to be exercised when making then.

Finally, whilst the use of Eq. 2 is widespread, it is instructive to point out that it has the tendency to reinforce the concept that individual lipid molecules have a certain defined shape. Extrapolating this ideal geometric lipid shape concept to the final organisation of lipid bilayers, comprising of lipids that prefer to form curved aggregates, has been argued to result in packing defects and voids [26]. However, one must not forget that lipid aggregates are dynamic systems and lipids are flexible molecules, which diffuse laterally through lipid aggregates. In such systems packing defects are likely averaged out as the flexibility of individual lipid molecules allows them to adapt to the local molecular environment.

1.2 The use of monolayer spontaneous curvature values in biological systems

Aside from academic interest in obtaining accurate c_0 values for lipids there has been much interest in constructing quantitative models of membrane protein regulation [2,20,27–29]. Lipid c_0 values have been widely used for this; they can be used to estimate the curvature elastic stress in bilayer membranes and relate this to protein activity [2,29,30]. Computational studies have also

established that stored curvature elastic stress regulates membrane lipid synthesis and many of these models have been parameterised by c_0 values available in the literature [10,31–35]. In a wider context, evidence suggests that some antineoplastic compounds target stored elastic energy in membranes [36,37] and oxidative stress of membranes can be mediated by membrane curvature elastic energy [38]. Furthermore, lipid nucleic acid interactions [39–41] are important in a number of contexts like gene delivery [42] and lipid curvature and the associated free energies play a role in understanding the mechanism behind lipid absorption in the intestines [43]. In these biological environments it is a challenge to determine whether a representative value of c_0 exists in the literature (i.e. measured under similar experimental conditions). This is less of an issue for temperature, since most studies have determined c_0 between room temperature and 37 °C, but more complicated for charged lipids, where c_0 values are ionic strength dependent.

When there is less interest in the absolute accuracy of c_0 values and more interest in consistency with an overall hypothesis, several rapid methods to determine c_0 values have also been reported. Typically such methods rely on the relationship between the swelling of the H_{II} phase and the relative c_0 values of a guest lipid in a well characterised host lipid [23], or pipette aspiration techniques [44]. The following data tables list c_0 values found in the literature, alongside key experimental details such as measurement temperature and buffer, the reader is recommended to refer to the original publications to understand any assumptions made in the calculation of c_0. Section 2.1 details the abbreviations used to describe the different lipids and buffer systems across all tables.

2.1 Terminology: abbreviations of buffers and lipids

The following abbreviations are used throughout, phosphatidylethanolamine (PE), phosphatidylcholine (PC), phosphatidylphosphate (PA), phosphatidylserine (PS), phosphatidylphosphoglycerol (PG), cardiolipin (CL), lysophosphatidylethanolamine (LPE), lysophosphatidylcholine (LPC), lysophosphatidylphosphate (LPA), lysophosphatidylserine (LPS), lysophosphatidylphosphoglycerol (LPG), diacylglycerol (DAG), monoacylglycerol (MAG), sphingomyelin (SM), diacylglyceryl-3-O-carboxyhydroxymethylcholine (DGCC), sulfoquinovosyl diacylglycerol SQDG, monoglucosyldiglyceride (MGDG) and phosphoglycerophosphate (PGP).

Other abbreviations used are N-nitrobenzoxadiazole (NBD), tetradecane (TD), dodecane (DD), tricosene (TS), N-[Tris(hydroxymethyl)methyl]-2-aminoethanesulfonic acid (TES), 2-(*N*-morpholino)ethanesulfonic acid (MES), (4-(2-hydroxyethyl)-1-piperazineethanesulfonic acid) (HEPES), Ethylenediaminetetraacetic acid (EDTA), piperazine-N,N'-bis(2-ethanesulfonic acid) (PIPES), tris(hydroxymethyl)aminomethane (TRIS) and 2-[Bis(2-hydroxyethyl)amino]-2-(hydroxymethyl)propane-1,3-diol (BIS TRIS).

Table 1 provides a key to each individual lipid and the abbreviations used to denote these lipids in this manuscript. The alkyl chain length, number of unsaturations and position of unsaturation is defined for all fatty acids, using the standard approach. Such that 18:1 (n=9) refers to a straight chain fatty acid with 18 carbons, 1 unsaturation, 9 carbons from the end of the alkyl chain. In this definition the *cis* configuration of the double bond and the acyl (ester) linkage to the glycerol is implicit. Alkyl (ether) linkages are defined by the letter *a* and *trans* isomers are defined by the letter *t*.

Accepted version: Chemistry and Physics of Lipids 239C (2021) 105117
Received 24 April 2021, Revised 3 July 2021, Accepted 9 July 2021, Available online 12 July 2021.

Table 1 Lipid abbreviations

Lipid name	Abbreviation
1,2-di-O-dodecyl-*sn*-glycero-3-phosphoethanolamine	D12aPE
1,2-dilauroyl-*sn*-glycero-3-phosphoethanolamine	DLPE
1,2-dimyristoyl-*sn*-glycero-3-phosphoethanolamine	DMPE
1,2-dipalmitoyl-*sn*-glycero-3-phosphoethanolamine	DPPE
1,2-diarachinoyl-*sn*-glycero-3-phosphoethanolamine	DAPE
1-palmitoyl-2-oleoyl-*sn*-glycero-3-phosphoethanolamine	POPE,
1,2-dipalmitoleoyl-*sn*-glycero-3-phosphoethanolamine	DiPoPE
1,2-dioleoyl-*sn*-glycero-3-phosphoethanolamine	DOPE
1,2-dielaidoyl-*sn*-glycero-3-phosphoethanolamine	DEPE
1,2-dipetroselinoyl-*sn*-glycero-3-phosphoethanaolamine	DPLPE
1,2-divaccenoyl-*sn*-glycero-3-phosphoethanolamine	DVPE
1-stearoyl-2-docosapentaenoyl-*sn*-glycero-3-phosphoethanolamine	SD5PE
1-stearoyl-2-docosahexaenoyl-*sn*-glycero-3-phosphoethanolamine	SD6PE
1,2-di-O-phytanyl-*sn*-glycero-3-phosphoethanolamine	DiPhyPE
1,2-dioleoyl-*sn*-glycero-3-phospho-N-methylethanolamine	DOPE-Me
1,2-dimyristoyl-*sn*-glycero-3-phosphoethanolamine-N-(7-nitro-2-1,3-benzoxadiazol-4-yl)	NBD-DMPE
1,2-dipalmitoyl-*sn*-glycero-3-phosphoethanolamine-N-(7-nitro-2-1,3-benzoxadiazol-4-yl)	NBD-DPPE
1,2-dioleoyl-*sn*-glycero-3-phosphoethanolamine-N-(7-nitro-2-1,3-benzoxadiazol-4-yl)	NBD-DOPE
1,2-didecanoyl-*sn*-glycerol-3-phosphocholine	DCPC
1,2-dilauroyl-*sn*-glycero-3-phosphocholine	DLPC
1,2-dimyristoyl-*sn*-glycero-3-phosphocholine	DMPC
1,2-dipalmitoyl-*sn*-glycero-3-phosphocholine	DPPC
1,2-distearoyl-*sn*-glycero-3-phosphocholine	DSPC
1-palmitoyl-2-oleoyl-*sn*-glycero-3-phosphocholine	POPC
1-stearoyl-2-oleoyl-*sn*-glycero-3-phosphocholine	SOPC
1,2-dioleoyl-*sn*-glycero-3-phosphocholine	DOPC
1,2-di-O-phytanoyl-*sn*-glycero-3-phosphocholine	DiPhyPC
1,2-di[(2'-hexyl)decanoyl]-*sn*-glycero-3-phosphocholine	PC (10,6)
1,2-di[(2'-octyl)dodecanoyl]-*sn*-glycero-3-phosphocholine	PC (12,8)
1,2-di[(2'-decyl)tetradecanoyl]-*sn*-glycero-3-phosphocholine	PC (14,10)
1,2-dioleoyl-*sn*-glycero-3-phosphate	DOPA
1,2-dioleoyl-*sn*-glycero-3-phospho-L-serine	DOPS
1,2-dioleoyl-*sn*-glycero-3-phospho-L-serine-N-(7-nitro-2-1,3-benzoxadiazol-4-yl)	NDB-DOPS
1-palmitoyl-2-oleoyl-*sn*-glycero-3-phospho-(1'-rac-glycerol)	POPG
1,2-dioleoyl-*sn*-glycero-3-phospho-(1'-rac-glycerol)	DOPG
tetraoleoylcardiolipin	TOCL
1-lauroyl-2-hydroxy-*sn*-glycero-3-phosphoethanolamine	L-LysoPE
1-palmitoyl-2-hydroxy-*sn*-glycero-3-phosphoethanolamine	P-LysoPE
1-stearoyl-2-hydroxy-*sn*-glycero-3-phosphoethanolamine	S-LysoPE
1-oleoyl-2-hydroxy-*sn*-glycero-3-phosphoethanolamine	O-LysoPE
1-lauroyl-2-hydroxy-*sn*-glycero-3-phosphocholine	L-LysoPC
1-palmitoyl-2-hydroxy-*sn*-glycero-3-phosphocholine	P-LysoPC
1-oleoyl-2-hydroxy-*sn*-glycero-3-phosphocholine	O-LysoPC
1-oleoyl-2-hydroxy-*sn*-glycero-3-phosphate	O-LysoPA
1-oleoyl-2-hydroxy-*sn*-glycero-3-phospho-L-serine-N-(7-nitro-2-1,3-benzoxadiazol-4-yl)	NBD-lysoOPS

1-myristoyl-2-hydroxy-*sn*-glycero-3-phosphoethanolamine-N-(7-nitro-2-1,3-benzoxadiazol-4-yl)	NBD-lysoMPE
1-palmitoyl-2-hydroxy-*sn*-glycero-3-phosphoethanolamine-N-(7-nitro-2-1,3-benzoxadiazol-4-yl)	NBD-lysoPPE
1-oleoyl-2-hydroxy-*sn*-glycero-3-phosphoethanolamine-N-(7-nitro-2-1,3-benzoxadiazol-4-yl)	NBD-lysoOPE
1,2-didecanoyl-*sn*-glycerol	DCG
1-2-dioleoyl-*sn*-glycerol	DOG
cholesterol	Chol
monoolein	MO
oleic acid	OA
elaidic acid	EA
alpha-Tocopherol	α-Toc
trans,trans-2,4-decanedienal	DD
cis-11-hexadecenal	HD
cis-retinal	cR
trans-retinal	tR
trans-retinoic acid	tRA
N-palmitoyl-D-erythro-sphingosylphosphorylcholine	PSM
egg sphingomyelin	ESM
N-acetoyl-D-erythro-sphingosine	C2:0 Cer
N-hexanoyl-D-erythro-sphingosine	C6:0 Cer
N-palmitoyl-D-erythro-sphingosine	C16:0 Cer
N-lignoceroyl-D-erythro-sphingosine	C24:0 Cer
diglucosyl dioleoylglycerol	DGlcDOG
glycerophosphoryldioleoylglycerol	GPDGlcDOG
monoglucosyldioleoylglycerol	MGlcDOG

2.2 Monolayer spontaneous curvature values of phosphatidylethanolamine lipids

Table 2 shows collected values of c_0 values for PE lipids. Due to their negative curvature preference, PE lipids tend to form H_{II} phases spontaneously, although shorter chain lipids require elevated temperatures to do this [45]. There is a general expectation that as the chain length of saturated lipids increases c_0 becomes more negative, reflecting the need to accommodate the molecular motions of the longer chains [46,47]. Due to their measurement at varying temperatures, different experimental conditions and at R_p or R_n, the values in Table 2 cannot be unambiguously used to quantify this relationship. However, as the unsaturated chain length increases, from 12 through to 16 carbons, c_0 becomes more negative. It is unclear if the levelling-off of c_0 seen for DAPE is an artefact of the high temperature of measurement or genuine behaviour. Figure 2A summarises this data.

Accepted version: Chemistry and Physics of Lipids 239C (2021) 105117
Received 24 April 2021, Revised 3 July 2021, Accepted 9 July 2021, Available online 12 July 2021.

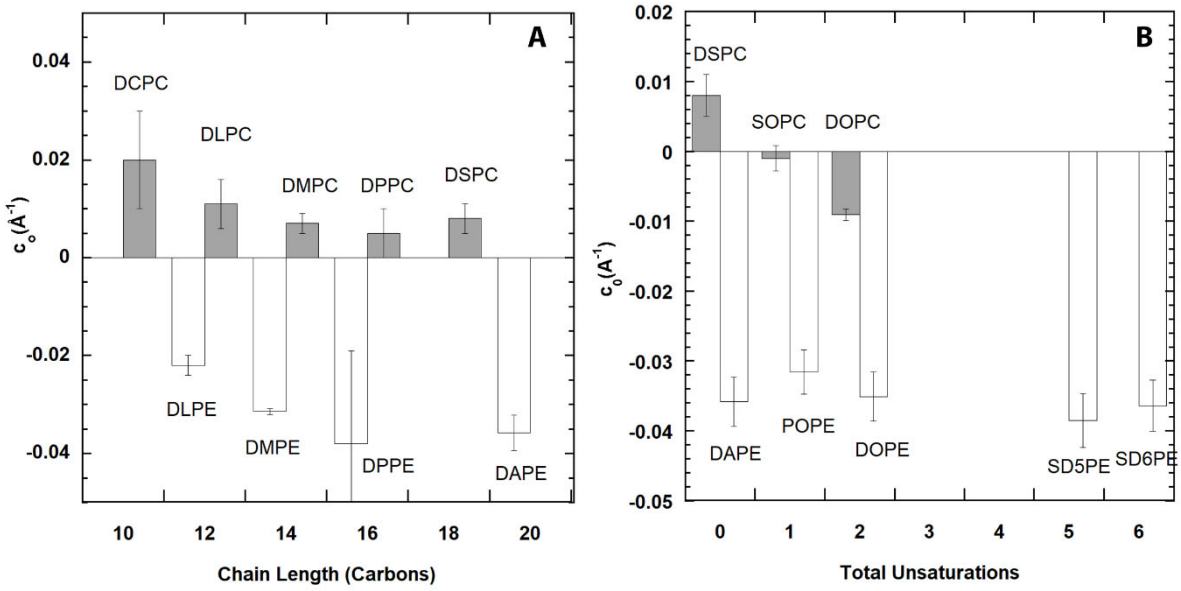

Figure 2 variation of c_0 with saturated diacyl chain length and unsaturation for PC and PE lipids. Figure 2A shows data for increasing saturated diacyl chain length and Figure 2B shows data for increasing unsaturation. PC lipids are shown in grey and PE lipids are shown in white. In the absence of an error bar in the published data a 10 % error was applied. Data values are shown in Tables 2 and 3.

Only a few monounsaturated PE lipids have had their c_0 value determined, which is a clear gap in the literature. More dimonounsaturated PE lipids, like DOPE, have had c_0 determined under a variety of different conditions, both at R_p and R_n. Values range from -0.0451 Å^{-1} at 90 °C [30] through to -0.0333 Å^{-1} [48]. The large range in values is probably a reflection of measurements at R_p or R_n, temperature variance and the effects of different buffers. Changing the position of unsaturation, but retaining overall chain length, keeps c_0 negative as does changing from *cis* to *trans* configuration, shown in Table 2 for DOPE, DEPE, DPLPE and DVPE. It should be noted that c_0 for DEPE was estimated for the purposes of this study using temperature dependent d_{hex} values [49] and the method of Dymond [23], with the assumption that the pivotal plane position of the 18:1*t* (n=9) DEPE chain is the same as for DOPE. The same assumption was made by Epand et al. [21] when determining c_0 for DPLPE and DVPE. Similarly, polyunsaturation in lipid chains retains the negative value of c_0, with c_0 values of SD5PE and SD6PE being similar to DOPE, obtained at the same temperature and conditions [50]. Both trends are expected and overall, there is a suggestion that c_0 decreases as the number of unsaturations increases, although the range of different conditions and different combinations of chain length used to obtain the data prevent quantitative comparisons across studies. It is perhaps surprising that SD5PE and SD6PE exhibit similar c_0 values to DAPE, but mismatch in the acyl chain lengths might explain this. Figure 2B shows this data comparing PE and PC lipids. DiPhyPE has the most negative c_0 of any PE lipid reported [23], which is consistent with the branching in the alkyl chain of this lipid, increasing the effective chain volume. Headgroup modifications such as methylation and the introduction of fluorescent labels influence PE c_0 values, but these lipids still retain their negative curvature preference.

The temperature dependence of c_0 for DOPE, DOPE-Me, DPLPE and DVPE lipids has been determined in several studies, indicated in Table 2. Values of c_0 for these PE lipids decrease as temperature increases, caused by the greater range of motion of the hydrocarbon chains with

Accepted version: Chemistry and Physics of Lipids 239C (2021) 105117
Received 24 April 2021, Revised 3 July 2021, Accepted 9 July 2021, Available online 12 July 2021.

elevated temperature. Over the temperature range of observation, these lipids all show linear dependence of c_0 on temperature, as summarised in Figure 3. Overall the data show that c_0 varies by about ± 10% over ± 25 °C, this is a comparatively small value but it is worth noting that the gradient changes with the position of unsaturation [21] and number of unsaturated acyl chains [18]. Chen et al. [51] have studied the temperature dependence of DOPE in a range of Ca^{2+} concentrations finding that the temperature dependence of c_0, like the c_0 of DOPE, is not influenced by Ca^{2+} concentration. All measured values of the c_0 dependence of DOPE are in agreement with values approximated from the temperature-driven swelling of the change in dimension of the DOPE H_{II} phase [52,53]. A detailed theoretical treatment has also been published [24].

Finally, careful examination of the c_0 values of DOPE in Table 2 suggests a small degree of buffer and pH dependence. Systematic studies show the effects of divalent cations are very small [51], but it is worth noting the range of c_0 values of DOPE reported across multiple studies might also be due to the effects of individual buffer interactions with the lipids [54].

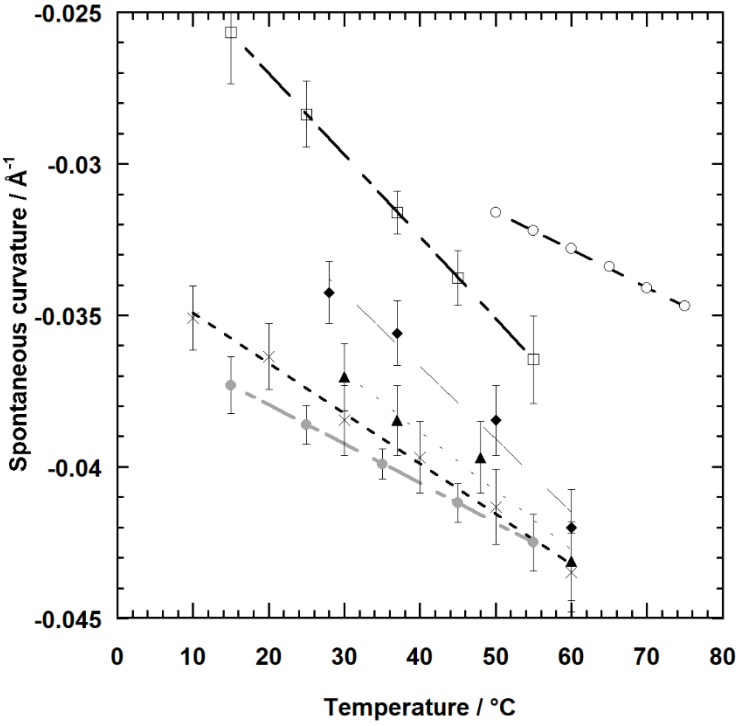

Figure 3 variation of c_0 with temperature for PE lipids. Grey circles and unfilled squares show data for DOPE and POPE, respectively (in water, TS) [18]. Grey crosses, filled triangles and filled diamonds show data for DOPE, DPLPE and DVPE respectively (in 2.0 mM TES, pH 7.4, TD) [21], data were extrapolated from graphs and error bars reflect resultant uncertainty. Unfilled circles show data for DOPE-Me (in water, DD) [55].

Accepted version: Chemistry and Physics of Lipids 239C (2021) 105117
Received 24 April 2021, Revised 3 July 2021, Accepted 9 July 2021, Available online 12 July 2021.

Table 2 Monolayer spontaneous curvature values of phosphatidylethanolamine lipids

Chains	Lipid	Matrix	c_0 (Å^{-1})	Buffer/ Components in mixture	T/ °C	Ref	dc_0/dT (Å^{-1}°C^{-1})
	saturated						
12:0a, 12:0a	D12aPE		-0.04801[e]	Water	135	[30]	
12:0, 12:0	DLPE		-0.022 ± 0.002[n]	Water, TS	35	[9]	
14:0, 14:0	DMPE		-0.0314 ± 0.0006[n]	Water, TS	80	[19]	
16:0, 16:0	DPPE		-0.0380 ± 0.0190[n]	20 mM Na_3PO_4, 130 mM NaCl, pH 7.4	35	[9]	
20:0, 20:0	DAPE		-0.0358[e]	Water	99	[30]	
	monounsaturated						
16:0, 18:1 (n=9)	POPE	DOPE	-0.0317 ± 0.0007[n]	Water, TS	35	[19]	
			-0.0350 ± 0.0070[n]	20 mM Na_3PO_4, 130 mM NaCl, pH 7.4	35	[20]	
			-0.0316 ± 0.0007[n]	Water, TS	37	[18][T]	-2.7 (± 0.7) x 10^{-4}
	dimonounsaturated						
16:1 16:1	DiPoPE		-0.0382 ± 0.0009	Water, TS	35	[19]	
			-0.037 ± 0.001	Water, TS	35	[56][T]	-1.7 x 10^{-4} [c]
18:1 (n=9), 18:1(n=9)	DOPE		-0.0353 ± 0.0025	2.0 mM TES, pH 7.4, TD	8	[21][T]	-1.7 x 10^{-4}
			-0.0342[e]	Water	10	[30]	
			-0.0333	Water, TD, pH 7.2	20	[48]	
			-0.0385	0.013 M HCl and 0.087 M KCl, TD, pH 2	20	[48]	
			-0.0331 ± 0.0009	10 mM HEPES, TD	20	[51][T]	-1.7 x 10^{-4} [c]
			-0.0340 ± 0.0009	10 mM HEPES, 10 mM $CaCl_2$, TD	20	[51][T]	-1.8 x 10^{-4} [c]
			-0.0342 ± 0.0008	10 mM HEPES, 30 mM $CaCl_2$, TD	20	[51][T]	-1.8 x 10^{-4} [c]
			-0.0343 ± 0.0009	10 mM HEPES, 50 mM $CaCl_2$, TD	20	[51][T]	-1.6 x 10^{-4} [c]
			-0.0343 ± 0.0009	10 mM HEPES, 70 mM $CaCl_2$, TD	20	[51][T]	-1.5 x 10^{-4} [c]
			-0.0347 ± 0.0009	10 mM HEPES, 100 mM $CaCl_2$, TD	20	[51][T]	-0.9 x 10^{-4} [c]
			-0.0420 ± 0.0048	Water	RT	[57]	
			-0.0444 ± 0.0020	Water, TD	RT	[57]	
			-0.0351	Water	22	[58]	
			-0.0340	Water, TD	22	[58]	

Accepted version: Chemistry and Physics of Lipids 239C (2021) 105117
Received 24 April 2021, Revised 3 July 2021, Accepted 9 July 2021, Available online 12 July 2021.

			-0.0370 ± 0.0013	Water, TD	22	[59]	
			-0.0435 ± 0.0018	25 mM TES, 25 mM MES, 150 mM NaCl, TD	22	[59]	
			-0.0455 ± 0.0020	25 mM TES, 25 mM MES, 150mM NaCl, 25 mM $CaCl_2$, TD	22	[59]	
			-0.0324	2 mM TES, TD	22	[14]	
			-0.0372 ± 0.0026	Water	30	[50]	
			-0.0399 ± 0.0005[n]	Water, TS	35	[18][T]	-1.3 (± 0.4) x 10^{-4}
			-0.0409 ± 0.0010[n]	Water, TS	35	[19]	
			-0.041 ± 0.001[n]	Water, TS	35	[56][T]	-1.6 x 10^{-4} [c]
			-0.0451[e]	Water	90	[30]	
18:1*t* (n=9), 18:1*t* (n=9)	DEPE		-0.0394[e]	Water	65	[49]	
18:1 (n=11), 18:1 (n=11)	DVPE		-0.0343 ± 0.0003	2.0 mM TES, pH 7.4, TD	28	[21][T]	-2.4 x 10^{-4} [c]
18:1 (n=6), 18:1 (n=6)	DPLPE		-0.0385 ± 0.0003	2.0 mM TES, pH 7.4, TD	37	[21][T]	-1.9 x 10^{-4} [c]
	polyunsaturated						
18:0, 22:5 (n=6)	SD5PE		-0.0385 ± 0.0027	Water	30	[50]	
18:0, 22:6 (n=3)	SD6PE		-0.0364 ± 0.0025	Water	30	[50]	
	Branched						
diphytanyl	DiPhyPE	DOPE	-0.0650 ± 0.0020	Water	27	[23]	
	Modified headgroups						
18:1 (n=9), 18:1(n=9)	DOPE-Me		-0.0316[n]	Water, DD	50	[55][T]	-1.3 x 10^{-4} [c]
14:0, 14:0	NBD-DMPE	EPC	−0.0310	150 mM NaCl, 50 mM HEPES, 2 mM EDTA	37	[60]	
16:0, 16:0	NBD-DPPE	EPC	−0.0220	150 mM NaCl, 50 mM HEPES, 2 mM EDTA	37	[60]	
18:1 (n=9), 18:1(n=9)	NBD-DOPE	EPC	−0.0310	150 mM NaCl, 50 mM HEPES, 2 mM EDTA	37	[60]	

[n] refers to studies where c_0 is measured at the neutral plane, [e] denotes an estimated value, [T] further temperature data available, [c] calculated for the purposes of this publication, using data in the cited study. Where errors are reported in the original publications these are reported. Abbreviations are defined in Table 1, Section 2.1.

Accepted version: Chemistry and Physics of Lipids 239C (2021) 105117
Received 24 April 2021, Revised 3 July 2021, Accepted 9 July 2021, Available online 12 July 2021.

2.3 Monolayer spontaneous curvature values of phosphatidylcholine lipids

PC lipids are generally bilayer-forming and depending on their molecular structure will likely exhibit weak positive or negative curvature. Values of c_0 for saturated diacylphosphatidylcholines, shown in Table 3, broadly support this. As the chain length increases from 10 to 18 carbons, these lipids express positive c_0 values, which decrease, shown in Figure 2A. It should be noted that a negative value of c_0 for DSPC has been reported [18] but a subsequent study by the same authors has revised this value [56]. Unsaturation in the alkyl chains promotes negative curvature in PC lipids, as shown in Figure 2B for DSPC, SOPC and DOPC. The introduction of branching in PC lipid hydrocarbon chains clearly promotes negative curvature to a magnitude comparable to that seen in DOPE [61]. For example, the branched lipid PC(10,6) has c_0 of -0.0392 $Å^{-1}$, which compares well with the values of DOPE shown in Table 2., whilst incorporating the phytanoyl alkyl chain also promotes negative curvature in PC lipids (-0.021 ± 0.001 $Å^{-1}$).

Temperature variance data of c_0 is available for PC lipids recalculated here from Kollmitzer et al. [18] and shown in Figure 4 and Table 3. As seen for PE lipids, there is a weak linear temperature dependence of c_0. In general, the gradient of c_0 temperature dependence differs slightly across the PC lipids studied i.e. SOPC, DOPC, DPPC, POPC and DSPC, however the overall errors in these studies [18] preclude any firm conclusions on how lipid chain length and unsaturation impact the temperature dependence of c_0. A recent updated study [56], further confirmed the weak temperature dependence of DPPC, POPC and DOPC c_0 values. The c_0 values of branched PC lipids have been measured at different temperatures and these also show weak temperature dependence, as shown in Table 3.

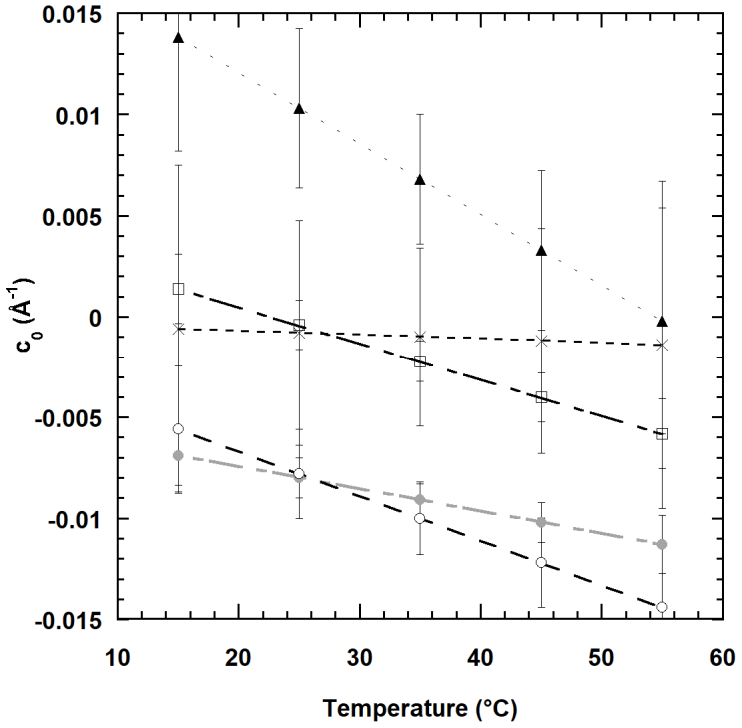

Figure 4 variation of c_0 with temperature for PC lipids. Filled (grey) circles, unfilled circles, unfilled squares, crosses and filled triangles show data for DOPC, SOPC, POPC, DSPC and DPPC respectively (in water, TS) [18].

Accepted version: Chemistry and Physics of Lipids 239C (2021) 105117
Received 24 April 2021, Revised 3 July 2021, Accepted 9 July 2021, Available online 12 July 2021.

Table 3 Monolayer spontaneous curvature values of phosphatidylcholine lipids

Chains	Lipid	Matrix	c_0 (Å^{-1})	Buffer/ Components in mixture	T/ °C	Ref	dc_0/dT (Å^{-1}°C^{-1})
	saturated						
10:0, 10:0	DCPC		0.0200 ± 0.0100^{e}		22	[62]	
12:0, 12:0	DLPC	DOPE	0.011 ± 0.005^{n}	Water, TS	35	[56]	
14:0, 14:0	DMPC		0.0250 ± 0.0100^{e}		22	[62]	
		DOPE	0.007 ± 0.002^{n}	Water, TS	35	[56]	
16:0,16:0	DPPC	DOPE	0.0068 ± 0.0032^{n}	Water, TS	35	[18]^{T}	-3.5 (± 2.3) x 10^{-4}
			0.005 ± 0.005^{n}	Water, TS	35	[56]T	-5.6 x 10^{-5} ^{c}
18:0, 18:0	DSPC	DOPE	-0.0100 ± 0.0044^{n}	Water, TS	35	[18]^{T}	-0.2 (± 3.4) x 10^{-4}
			0.008 ± 0.003^{n}	Water, TS	35	[56]	
	monounsaturated						
16:0, 18:1	POPC	DOPE	-0.0022 ± 0.0010^{n}	Water, TS	35	[18]^{T}	-1.8 (± 0.7) x 10^{-4}
			0.001 ± 0.004^{n}	Water, TS	35	[56]T	-1.1 x 10^{-4} ^{c}
18:0, 18:1	SOPC	DOPE	-0.0010 ± 0.0018^{n}	Water, TS	35	[18]^{T}	-2.2 (± 1.3) x 10^{-4}
	dimonounsaturated						
18:1 (n=9), 18:1(n=9)	DOPC		-0.0115	Water, TD	32	[58]	
	DOPC	DOPE	-0.0091 ± 0.0008^{n}	Water, TS	35	[18]^{T}	-1.1 (± 0.6) x 10^{-4}
			-0.004 ± 0.004^{n}	Water, TS	35	[56]T	-5.8 x 10^{-5} ^{c}
	Branched						
diphytanoyl	DiPhyPC	DOPE	-0.021 ± 0.001^{n}	Water, TS	35	[56]T	1.5 x 10^{-4} ^{c}
1,2-di[(2'-hexyl)decanoyl]	PC(10,6)		-0.0392	20 mM PIPES, 1 mM EDTA, 150 mM NaCl, 0.002% NaN_3, pH 7.4, TD	25	[61]T	-4.6 x 10^{-5} ^{c}
1,2-di[(2'-octyl)dodecanoyl]	PC(12,8)		-0.0351	20 mM PIPES, 1 mM EDTA, 150 mM NaCl, 0.002% NaN_3, pH 7.4, TD	25	[61]T	-2.9 x 10^{-5} ^{c}
1,2-di[(2'-decyl)tetradecanoyl]	PC(14,10)		-0.0339	20 mM PIPES, 1 mM EDTA, 150 mM NaCl, 0.002% NaN_3, pH 7.4, TD	25	[61]T	-1.86 x 10^{-5} ^{c}

Accepted version: Chemistry and Physics of Lipids 239C (2021) 105117
Received 24 April 2021, Revised 3 July 2021, Accepted 9 July 2021, Available online 12 July 2021.

^{n} refers to studies where c_0 is measured at the neutral plane, ^{e} denotes an estimated value, ^{T} further temperature data available, ^{c} calculated for the purposes of this publication, using data in the cited study. Where errors are reported in the original publications these are reported. Abbreviations are defined in Table 1, Section 2.1.

Accepted version: Chemistry and Physics of Lipids 239C (2021) 105117
Received 24 April 2021, Revised 3 July 2021, Accepted 9 July 2021, Available online 12 July 2021.

2.4 Monolayer spontaneous curvature values of anionic phospholipids

The c_0 values of anionic phospholipids are very sensitive to the concentration of monovalent and divalent ions under the conditions of measurement. This is thought to be through a mixture of electrostatic screening, which has been modelled using non-linear Possion-Boltzmann theory by Lekkerkerker [63], and the bridging effects of divalent cations; pH is also likely to significantly impact their c_0 value.

In comparison to the zwitterionic lipids, relatively few c_0 values for anionic lipids like PA, PS, CL and PG lipids have been determined. Values that have been obtained are for the acyl chain combinations of the most abundant lipids in mammalian cells i.e., 18:1,18:1 or 16:0,18:1. Table 4 shows values of c_0 for these anionic lipids, which suggest significant counterion dependence. DOPA lipids show negative c_0 values, which range from -0.0077 $Å^{-1}$ in water through to -0.0312 ± 0.0043, induced by 100 mM $CaCl_2$. The concentration dependence of the c_0 of DOPA in $CaCl_2$ is linear, varying at 0.21 $Å^{-1}M^{-1}$ [51]. The temperature dependence studies available suggest that c_0 values of DOPA do not vary within error, data are shown in Table 4. This is attributed to increases in thermal motion of the acyl chains being offset by temperature-dependent electrostatic effects [51]. In water, DOPS exhibits positive curvature of 0.0069 $Å^{-1}$, thought to be caused by inter headgroup repulsions, but tight negative curvatures are induced by low pH (-0.0435 $Å^{-1}$). Interestingly, modification of DOPS by the fluorescent NBD headgroup appears to give a negative curvature preference. The authors attribute this to the conditions of experiment, notably the low composition of NBD-DOPS studied in the membrane, which means inter-headgroup repulsion between NBD-DOPS molecules could not occur [60].

Similar behaviour has been observed for low concentrations of DOPS and DOPA lipids in a DOPE H_{II} matrix, presenting evidence that c_0 values of DOPS and DOPA at pH 7.0 are dependent on the competing effects of headgroup repulsion and bridging ions [23]. The range of c_0 values for this study, shown in Table 4, supports the idea that headgroup-headgroup repulsion drives positive curvature in DOPA and DOPS systems. When the concentration of these anionic lipids is too low for headgroup-headgroup repulsion to dominate, or divalent cations are abundant enough for bridging effects to occur, DOPS and DOPA have negative spontaneous curvatures, as modelled using kinetic equilibria by the authors [23]. Observations like this raise interesting questions as to what the spontaneous curvature of anionic lipids is *in vivo*, since it is hard to determine *in vivo* concentrations of cations. Furthermore, these observations suggest that a degree of caution needs to be exercised when selecting c_0 values for enzyme assays that inevitably change the ratio of anionic lipids to divalent cations in different studies. There appear to be no studies of the temperature dependence of c_0 for PS lipids.

Currently there are only a few studies quantifying the c_0 of PG lipids, these focus on DOPG and show that it is also sensitive to divalent cations concentration but overall, the range of curvatures achieved is less than for DOPS or DOPA. The temperature dependence of c_0 for PG lipids has not been determined. Similarly, there are limited studies of the c_0 of CL lipids. TOCL shows weak positive curvature ($c_0 \approx 0$) in the absence of divalent cations and c_0 varies linearly at 0.14 $Å^{-1}M^{-1}$ with increasing $CaCl_2$, inducing moderate negative c_0 values. As for DOPA, the c_0 values of TOCL show no temperature dependence, due to the increasing range of thermal motions in the hydrocarbon chains being offset by changes to the electrostatics of the headgroups [51]. Since this behaviour has been seen in DOPA and TOCL it is likely that no temperature dependence will be seen for the c_0 values of other anionic lipids. This behaviour is expected to be dependent on the charge state of these lipids under the conditions of study. Finally, it is worth pointing out that no c_0 values for

Accepted version: Chemistry and Physics of Lipids 239C (2021) 105117
Received 24 April 2021, Revised 3 July 2021, Accepted 9 July 2021, Available online 12 July 2021.

phosphatidylinositol lipids could be identified in the literature although studies suggest these lipids promote negative curvature [64].

Accepted version: Chemistry and Physics of Lipids 239C (2021) 105117
Received 24 April 2021, Revised 3 July 2021, Accepted 9 July 2021, Available online 12 July 2021.

Table 4 Monolayer spontaneous curvature values of anionic phospholipids

Chains	Lipid	Matrix	c_0 (Å^{-1})	Buffer/ Components in mixture	T/ °C	Ref	dc_0/dT (Å^{-1}°C^{-1})
	PA						
18:1 (n=9), 18:1(n=9)	DOPA	DOPE	-0.0077	Water, TD	22	[59]	
		DOPE	-0.0217	25 mM TES, 25 mM MES, 150 mM NaCl, TD	22	[59]	
		DOPE	-0.0233	25 mM TES, 25 mM MES, 150 mM NaCl, 25 mM $CaCl_2$, TD	22	[59]	
		DOPE	-0.0106 ± 0.0039	10 mM HEPES, TD	20	[51]^r	-1.5 x 10^{-5} ^{c}
		DOPE	-0.0122 ± 0.0195	10 mM HEPES, 10 mM $CaCl_2$, TD	20	[51]^r	4.0 x 10^{-4} ^{c}
		DOPE	-0.0233 ± 0.0074	10 mM HEPES, 50 mM $CaCl_2$, TD	20	[51]^r	1.0 x 10^{-4} ^{c}
		DOPE	-0.0249 ± 0.0032	10 mM HEPES, 70 mM $CaCl_2$, TD	20	[51]^r	2.0 x 10^{-5} ^{c}
		DOPE	-0.0312 ± 0.0043	10 mM HEPES, 100 mM $CaCl_2$, TD	20	[51]^r	8.0 x 10^{-5} ^{c}
		DOPE	-0.043 ± 0.003 to -0.034 ± 0.003^e	Water	37	[23]	
		DOPE	-0.042 ± 0.003 to -0.031 ± 0.002^e	150 mM BIS TRIS, 10 mM $MgCl_2$ and 3 mM $CaCl_2$ at pH 7.0	37	[23]	
		DOPE	-0.068 ± 0.005 to -0.042 ± 0.003^e	150 mM BIS TRIS, 50 mM $MgCl_2$ and 15 mM $CaCl_2$ at pH 7.0	37	[23]	
		DOPE	-0.054 ± 0.003 to -0.045 ± 0.004^e	150 mM BIS TRIS, 100 mM $MgCl_2$, and 30 mM $CaCl_2$ at pH 7.0	37	[23]	
	PS						
18:1 (n=9), 18:1(n=9)	DOPS	DOPE	0.0069	Water, TD, pH 7.2	20	[48]	
		DOPE	-0.0435	13 mM HCl and 87 mM KCl, TD, pH 2	20	[48]	
		DOPE	-0.041 ± 0.003 to -0.026 ± 0.002^e	Water	37	[23]	
		DOPE	-0.041 ± 0.003 to -0.014 ± 0.001^e	150 mM BIS TRIS, 10 mM $MgCl_2$ and 3 mM $CaCl_2$ at pH 7.0	37	[23]	
		DOPE	-0.049 ± 0.004 to -0.041 ± 0.003^e	150 mM BIS TRIS, 50 mM $MgCl_2$ and 15 mM $CaCl_2$ at pH 7.0	37	[23]	

Accepted version: Chemistry and Physics of Lipids 239C (2021) 105117
Received 24 April 2021, Revised 3 July 2021, Accepted 9 July 2021, Available online 12 July 2021.

		DOPE	-0.043 ± 0.003 to -0.042 ± 0.003[e]	150 mM BIS TRIS, 100 mM $MgCl_2$, and 30 mM $CaCl_2$ at pH 7.0	37	[23]	
	NBD-DOPS	EPC	-0.0420	150 mM BIS TRIS, NaCl, 50 mM HEPES, 2 mM EDTA	37	[60]	
	PG						
16:0, 18:1	POPG		0.0020 ± 0.0030[n]	20 mM Na_3PO_4, 130 mM NaCl, pH 7.4	35	[20]	
18:1 (n=9), 18:1(n=9)	DOPG		0.0030 ± 0.0060[n]	20 mM Na_3PO_4, 130 mM NaCl, pH 7.4	35	[9]	
			-0.0124 ± 0.0037	50 mM TRIS, 150 mM NaCl, 20 mM $MgCl_2$, TS, pH 7.4	40	[22]	
			-0.0007 ± 0.0021	50 mM TRIS, 150 mM NaCl, TS, pH 7.4	40	[22]	
	CL						
18:1 (n=9), 18:1(n=9), 18:1 (n=9), 18:1(n=9)	TOCL	DOPE	2.27×10^{-4} ± 0.0066	10 mM HEPES, TD	20	[51][T]	2.1×10^{-5} [c]
		DOPE	-0.0040 ± 0.0083	10 mM HEPES, 10 mM $CaCl_2$, TD	20	[51][T]	1.5×10^{-5} [c]
		DOPE	-0.0036 ± 0.0091	10 mM HEPES, 20 mM $CaCl_2$, TD	20	[51][T]	9.5×10^{-5} [c]
		DOPE	-0.0090 ± 0.0055	10 mM HEPES, 50 mM $CaCl_2$, TD	20	[51][T]	1.5×10^{-5} [c]
		DOPE	-0.0146 ± 0.0022	10 mM HEPES, 100 mM $CaCl_2$, TD	20	[51][T]	-2.0×10^{-4} [c]

[n] refers to studies where c_0 is measured at the neutral plane, [e] denotes an estimated value, [T] further temperature data available, [c] calculated for the purposes of this publication, using data in the cited study. Where errors are reported in the original publications these are reported. Abbreviations are defined in Table 1, Section 2.1.

Accepted version: Chemistry and Physics of Lipids 239C (2021) 105117
Received 24 April 2021, Revised 3 July 2021, Accepted 9 July 2021, Available online 12 July 2021.

2.5 Monolayer spontaneous curvature values of lysophospholipids, acylglycerols, fatty acids, fatty aldehydes and miscellaneous lipids

Table 5 shows the c_0 values for lysophospholipids and acylglycerols. All the lyso phospholipid species studied exhibit positive c_0 values, which is expected given that these single chain lipids have a narrower cross-sectional area than their diacyl analogues. The c_0 values of lyso PS lipids do not appear to have been determined. Fluorescent NBD-labelled lysolipids have been studied and c_0 values for these broadly match their non-fluorescent counterparts. Diacylglycerol (DAG) and monoacylglycerol (MAG) lipids exhibit negative c_0 values, at least at the chain lengths studied. This makes MO the only lysolipid with a negative c_0 value. Table 6 shows the c_0 values of a range of other lipid species that have been determined. Figure 5 shows the different c_0 values reported for the dioleoyl chain configuration with different headgroups, comparing the c_0 of DOG to the range of DOG-containing lipids.

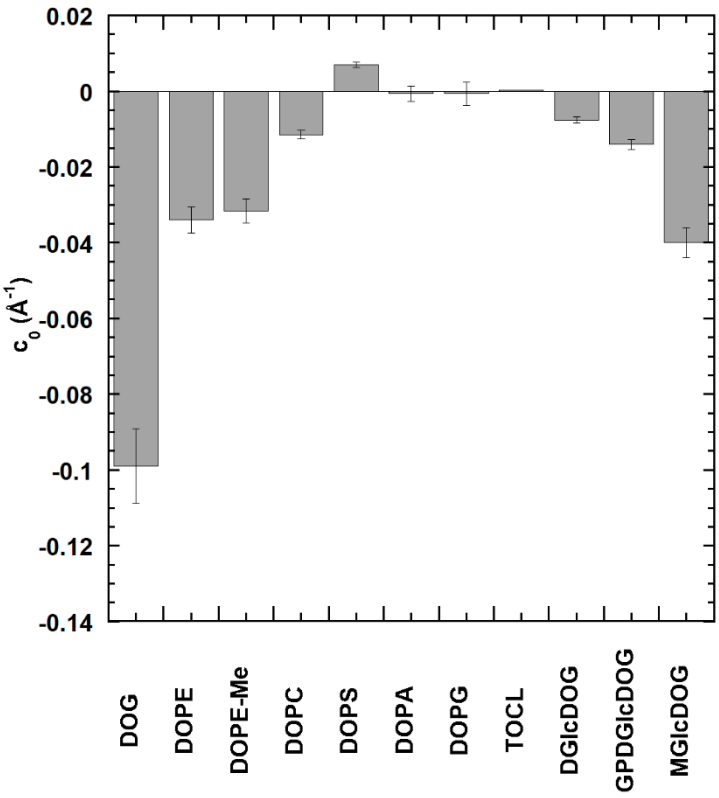

Figure 5 the variation of c_0 with lipid headgroup structure. All data show oleoyl chains with c_0 values measured in water, TD (except DOPG and TOCL, measured in buffer, see Table 3). DOG data included for completeness.

It is also worth pointing out the c_0 values of other lipids that have been determined, shown in Table 6, since these are often of biological significance. Cholesterol is a major component of eukaryotic cells, which has a negative c_0 value (-0.037 to -0.094 $Å^{-1}$), depending on measurement conditions. The c_0 of cholesterol, like zwitterionic lipids, is weakly temperature-dependent (-3.5 ± 0.9 x 10^{-4} $Å^{-1}°C^{-1}$) [18]. Other lipids that have had c_0 quantified are the fatty acids and fatty aldehydes i.e. OA, EA, DD, HD, retinal and retinoic acid which all show tight negative curvatures [23]. Many of these compounds, notably αToc (vitamin E) [65] are of importance in oxidative stress/ lipid

Accepted version: Chemistry and Physics of Lipids 239C (2021) 105117
Received 24 April 2021, Revised 3 July 2021, Accepted 9 July 2021, Available online 12 July 2021.

peroxidation pathways [38]. Ceramide lipids also show negative c_0 values and as anticipated increasing the second alkyl chain length decreases c_0 [56]. Studies of the temperature dependence of c_0 for the ceramides show c_0 decreases with temperature to an extent comparable with cholesterol. Finally, the glycolipids DGlcDOG, GPDGlcDOG and MGlcDOG all have negative c_0 values. Of particular note is the observation that MGlcDOG has a similar c_0 to DOPE, which adds a degree of quantitative rigour to understanding studies that have shown MGDG lipids can substitute for PE lipids in *Escherichia coli* [66]. The significance of this observation is that MGDG lipids are not found in *E. coli* so these observations support the intrinsic curvature hypothesis, as modelled in *Acholeplasma laidlawii* [35].

Accepted version: Chemistry and Physics of Lipids 239C (2021) 105117
Received 24 April 2021, Revised 3 July 2021, Accepted 9 July 2021, Available online 12 July 2021.

Table 5 Monolayer spontaneous curvature values of lyso phospholipids and acylglycerols

Chains	Lipid	Matrix	c_0 (Å^{-1})	Buffer/ Components in mixture	T/ °C	Ref
	LPE					
12:0	L-lysoPE	DOPE	>0.0025	Water, TD	22	[67]
16:0	P-lysoPE		0.0180 ± 0.0123[n]	20 mM Na_3PO_4, 130 mM NaCl, pH 7.4	35	[20]
18:0	S-lysoPE	DOPE	>0.0025	Water, TD	22	[67]
18:1(n=9)	O-lysoPE	DOPE	>0.0025	Water, TD	22	[67]
	LPC					
12:0	L-lysoPC	DOPE	0.0172	Water, TD	22	[67]
16:0	P-lysoPC	DOPE	0.0147	Water, TD	22	[67]
18:1(n=9)	O-lysoPC	DOPE	0.0263	Water, TD	22	[67]
	LPA					
18:1(n=9)	O-lysoPA	DOPE	0.0500	Water, TD	22	[59]
		DOPE	0.0500	25 mM TES, 25 mM MES, 150 mM NaCl, TD	22	[59]
		DOPE	0.0435	25 mM TES, 25 mM MES, 150 mM NaCl, 25 mM $CaCl_2$, TD	22	[59]
	Modified headgroups					
	LPS					
18:1(n=9)	NBD-O-lysoPS	EPC	−0.001	150 mM NaCl, 50 mM HEPES, 2 mM EDTA	37	[60]
	LPE					
14:0	NBD-M-lysoPE	EPC	0.0270	150 mM NaCl, 50 mM HEPES, 2 mM EDTA	37	[60]
16:0	NBD-P-lysoPE	EPC	0.0170	150 mM NaCl, 50 mM HEPES, 2 mM EDTA	37	[60]
18:1(n=9)	NBD-O-lysoPE	EPC	0.0010	150 mM NaCl, 50 mM HEPES, 2 mM EDTA	37	[60]
	DAG					
10:0, 10:0	DCG	DOPE	-0.07519	Water, TD	22	[68]
18:1(n=9), 18:1(n=9)	DOG	DOPC	-0.09901	Water, TD	22	[68]
	DOG	DOPE	-0.08696	2 mM TES, pH 7.4	22	[69]
	MAG					
18:1(n=9)	MO	DOPE	-0.054 ± 0.0030 [e]	Water	27	[23]

Accepted version: Chemistry and Physics of Lipids 239C (2021) 105117
Received 24 April 2021, Revised 3 July 2021, Accepted 9 July 2021, Available online 12 July 2021.

^{n} refers to studies where c_0 is measured at the neutral plane, ^{e} denotes an estimated value. Where errors are reported in the original publications these are reported. Abbreviations are defined in Table 1, Section 2.1.

Accepted version: Chemistry and Physics of Lipids 239C (2021) 105117
Received 24 April 2021, Revised 3 July 2021, Accepted 9 July 2021, Available online 12 July 2021.

Table 6 Monolayer spontaneous curvature values of fatty acids, fatty aldehydes and miscellaneous lipids

Chains	Lipid	Matrix	c_0 (Å^{-1})	Buffer/ Components in mixture	T/ °C	Ref	dc_0/dT (Å^{-1}°C^{-1})
	Sterols						
	chol	DOPE	-0.0439	Water	22	[58]	
		DOPC	-0.0368	Water	32	[58]	
		DOPE	-0.0940 ± 0.0013[n]	Water, TS	35	[18][T]	-3.5 (± 0.9) x 10^{-4}
		DOPE	-0.0470 ± 0.0050	Water	27	[23]	
	Aldehydes and acids						
18:1(n=9)	OA	DOPE	-0.0710 ± 0.0300	Water	27	[23,70]	
18:1t(n=9)	EA	DOPE	-0.0641[e]	20 mM HEPES, pH 7.4,	40	[23]	
	DD	DOPE	-0.0630 ± 0.0500	Water	27	[23,71]	
	HD	DOPE	-0.0520 ± 0.0400	Water	27	[23,71]	
	cR	DOPE	-0.1130 ± 0.0600	Water	27	[23]	
	tR	DOPE	-0.1050 ± 0.1600	Water	27	[23]	
	tRA	DOPE	-0.0630 ± 0.0400	Water	27	[23]	
	Ceramides						
d18:1/2:0	C2:0 Cer	DOPE	-0.03 ± 0.02	Water, TS	35	[56][T]	-4.2 x 10^{-5} [c]
d18:1/6:0	C6:0 Cer	DOPE	-0.09 ± 0.02	Water, TS	35	[56][T]	-2.5 x 10^{-4} [c]
d18:1/16:0	C16:0 Cer	DOPE	-0.11 ± 0.02	Water, TS	35	[56][T]	-2.4 x 10^{-4} [c]
d18:1/24:0	C24:0 Cer	DOPE	-0.15 ± 0.03	Water, TS	50	[56][T]	-3.6 x 10^{-4} [c]
	Other lipids						
	α-Toc	DOPE	-0.0730	Water	22	[72]	

Accepted version: Chemistry and Physics of Lipids 239C (2021) 105117
Received 24 April 2021, Revised 3 July 2021, Accepted 9 July 2021, Available online 12 July 2021.

	ESM	DOPE	-0.0134 ± 0.0072[n]	Water, TS	35	[18][T]	1.4 (± 5.1) x 10^{-4} *
	PSM	DOPE	0.010 ± 0.006[n]	Water, TS	35	[56][T]	-4.2 x 10^{-5} [c]
18:1(n=9), 18:1(n=9)	DGlcDOG		-0.0076[e]	Water	40	[35]	
18:1(n=9), 18:1(n=9)	GPDGlcDOG		-0.0130[e]	Water	40	[35]	
18:1(n=9), 18:1(n=9)	MGlcDOG		-0.0400[e]	Water	40	[35]	

[n] refers to studies where c_0 is measured at the neutral plane, [e] denotes an estimated value, [T] further temperature data available, [c] calculated for the purposes of this publication, using data in the cited study. Where errors are reported in the original publications these are reported. Abbreviations are defined in Table 1, Section 2.1, * see original study, authors suspect phase separation.

Accepted version: Chemistry and Physics of Lipids 239C (2021) 105117
Received 24 April 2021, Revised 3 July 2021, Accepted 9 July 2021, Available online 12 July 2021.

Conclusions

Estimates suggest many tens of thousands of different lipid species exist in nature. To date only a handful of these have had c_0 values determined. Given the enormity of the task to determine c_0 for all lipids, it is likely that c_0 for most lipids will always remain undetermined. Realistically, given this limitation, the best-case scenario is probably one where models of the variance of c_0 with unsaturation, chain length and other physical properties are refined to enable c_0 values of lipids to be estimated from other properties. There are a few examples of this such as the curvature power concept [23], and computational methods offer an alternative [73]. However, to develop such models further, the experimental determination of c_0 for some 'missing' lipids is still needed. These lipids are now pointed out. For the most part the dominant eukaryotic lipid headgroup classes have all had c_0 values determined, except for PI. The focus in nearly all studies has been on the dioleoyl chain configuration and further detail of the effect of unsaturation and chain length on c_0 is needed. Such studies would be most useful if they focused on the fatty acid chain configurations found in mammalian cells, particularly those featuring polyunsaturated fatty acids. Similarly, the c_0 values of the corresponding free fatty acids would also be a useful addition.

It would also be useful to expand the range of lipid headgroup classes that c_0 is reported for. So, for example, there are no c_0 values for betaine lipids like DGCC, SQDG in the literature, these would be an useful addition since it has been suggested under conditions of phosphorous starvation DGCC replaces PC lipids in diatoms and other species [74]. The lipids of extremophiles are another interesting area where few c_0 values appear to exist, especially at the molar concentration that appear to define the limits of life. Some useful additions would be c_0 values for lipids found in extremophiles [75] such as PGP lipids, more phytanyl/ phytanoyl lipids and macrocyclic archaeol, although the difficulty of obtaining these lipids as pure compounds can be a limiting factor.

Some studies have looked at the impact of temperature on c_0, however further studies in this area are needed to pin down whether all lipid alkyl chain combinations behave similarly, or as the data in Figures 3 and 4 suggest, the temperature dependence of c_0 is unsaturation and chain length dependent. Finally, the effect of pressure on c_0 does not appear have been studied in any detail although it is anticipated that high pressure will impact the mechanical properties of lipid bilayers [76]. Obtaining such data will likely expand our understanding of mechanism that cells employ to survive in extreme environments and may perhaps contribute to a more quantitative understanding of the physical limits of life.

Accepted version: Chemistry and Physics of Lipids 239C (2021) 105117
Received 24 April 2021, Revised 3 July 2021, Accepted 9 July 2021, Available online 12 July 2021.

References

1. Helfrich W. 1973 Elastic properties of lipid bilayers: theory and possible experiments. *Z. Naturforsch. C.* **28**, 693–703. (doi:10.1002/mus.880040211)

2. Attard GS, Templer RH, Smith WS, Hunt AN, Jackowski S. 2000 Modulation of CTP:phosphocholine cytidylyltransferase by membrane curvature elastic stress. *Proc. Natl. Acad. Sci. U. S. A.* **97**, 9032–9036. (doi:10.1073/pnas.160260697)

3. Zimmerberg J, Kozlov MM. 2006 How proteins produce cellular membrane curvature. *Nat. Rev. Mol. Cell Biol.* **7**, 9–19. (doi:10.1038/nrm1784)

4. Gruner SM. 1985 Intrinsic curvature hypothesis for biomembrane lipid composition: a role for nonbilayer lipids. *Proc. Natl. Acad. Sci. U. S. A.* **82**, 3665–3669.

5. McMahon HT, Gallop JL. 2005 Membrane curvature and mechanisms of dynamic cell membrane remodelling. *Nature* **438**, 590–596. (doi:10.1038/nature04396)

6. Callan-Jones A, Sorre B, Bassereau P. 2011 Curvature-driven lipid sorting in biomembranes. *Cold Spring Harb. Perspect. Biol.* **3**, 1–14. (doi:10.1101/cshperspect.a004648)

7. Bhatia T, Christ S, Steinkühler J, Dimova R, Lipowsky R. 2020 Simple sugars shape giant vesicles into multispheres with many membrane necks. *Soft Matter* **16**, 1246–1258. (doi:10.1039/c9sm01890e)

8. Steinkühler J, Knorr RL, Zhao Z, Bhatia T, Bartelt SM, Wegner S, Dimova R, Lipowsky R. 2020 Controlled division of cell-sized vesicles by low densities of membrane-bound proteins. *Nat. Commun.* **11**, 1–11. (doi:10.1038/s41467-020-14696-0)

9. Semeraro EF, Marx L, Frewein MPK, Pabst G. 2021 Increasing complexity in small-angle X-ray and neutron scattering experiments: From biological membrane mimics to live cells. *Soft Matter* **17**, 222–232. (doi:10.1039/c9sm02352f)

10. Dymond MK, Hague C V, Postle AD, Attard GS. 2013 An in vivo ratio control mechanism for phospholipid homeostasis: evidence from lipidomic studies. *J. R. Soc. Interface* **10**, 20120854. (doi:10.1098/rsif.2012.0854)

11. Deserno M. 2014 Fluid lipid membranes: From differential geometry to curvature stresses. *Chem. Phys. Lipids* **185**, 11–45. (doi:10.1016/j.chemphyslip.2014.05.001)

12. Marsh D. 2013 *Handbook of lipid bilayers*. CRC Press.

13. Kozlov MM. 2007 Determination of lipid spontaneous curvature from X-ray examinations of inverted hexagonal phases. *Methods Mol. Biol.* **400**, 355–66. (doi:10.1007/978-1-59745-519-0_24)

14. Rand RP, Fuller NL, Gruner SM, Parsegian VA. 1990 Membrane Curvature, Lipid Segregation, and Structural Transitions for Phospholipids under Dual-Solvent Stress. *Biochemistry* **29**, 76–87. (doi:10.1021/bi00453a010)

15. Chen Z, Rand RP. 1998 Comparative study of the effects of several n-alkanes on phospholipid hexagonal phases. *Biophys. J.* **74**, 944–952. (doi:10.1016/S0006-3495(98)74017-2)

16. Sjölund M, Rilfors L, Lindblom G. 1989 Reversed Hexagonal Phase Formation in Lecithin–Alkane–Water Systems with Different Acyl Chain Unsaturation and Alkane Length. *Biochemistry* **28**, 1323–1329. (doi:10.1021/bi00429a057)

17. Kozlov MM, Winterhalter M. 1991 Elastic moduli for strongly curved monolayers. Position of the neutral surface. *J. Phys. II* **1**, 1077–1084. (doi:10.1051/jp2:1991201)

18. Kollmitzer B, Heftberger P, Rappolt M, Pabst G. 2013 Monolayer spontaneous curvature of raft-forming membrane lipids. *Soft Matter* **9**, 10877. (doi:10.1039/c3sm51829a)

19. Frewein MPK, Rumetshofer M, Pabst G. 2019 Global small-angle scattering data analysis of inverted hexagonal phases. *J. Appl. Crystallogr.* **52**, 403–414. (doi:10.1107/S1600576719002760)

20. Leber R, Pachler M, Kabelka I, Svoboda I, Enkoller D, Vácha R, Lohner K, Pabst G. 2018 Synergism of Antimicrobial Frog Peptides Couples to Membrane Intrinsic Curvature Strain. *Biophys. J.* **114**, 1945–1954. (doi:10.1016/j.bpj.2018.03.006)

21. Epand RM, Fuller N, Rand RP. 1996 Role of the position of unsaturation on the phase behavior and intrinsic curvature of phosphatidylethanolamines. *Biophys. J.* **71**, 1806–1810. (doi:10.1016/S0006-3495(96)79381-5)

22. Alley SH, Ces O, Barahona M, Templer RH. 2008 X-ray diffraction measurement of the monolayer spontaneous curvature of dioleoylphosphatidylglycerol. *Chem. Phys. Lipids* **154**, 64–67. (doi:10.1016/j.chemphyslip.2008.03.007)

23. Dymond MK, Gillams RJ, Parker DJ, Burrell J, Labrador A, Nylander T, Attard GS. 2016 Lipid Spontaneous Curvatures Estimated from Temperature-Dependent Changes in Inverse Hexagonal Phase Lattice Parameters: Effects of Metal Cations. *Langmuir* **32**, 10083–10092. (doi:10.1021/acs.langmuir.6b03098)

24. Marsh D. 1996 Intrinsic curvature in normal and inverted lipid structures and in membranes. *Biophys. J.* **70**, 2248–55. (doi:10.1016/S0006-3495(96)79790-4)

25. A.J. Sodt, Venable RM, Lyman E, Pastor RW. 2016 Non-additive compositional curvature energetics of lipid bilayers. *Phys Rev Lett* **117**, 138104. (doi:doi:10.1103/PhysRevLett.117.138104)

26. Sadoc JF, Charvolin J. 1986 Frustration in bilayers and topologies of liquid crystals of amphiphilic molecules. *J. Phys. Fr.* **47**, 683–691. (doi:DOI: 10.1051/jphys:01986004704068300)

27. Wei Y, Mayoral-Delgado I, Stewart NA, Dymond MK. 2019 Macromolecular crowding and membrane binding proteins: The case of phospholipase A1. *Chem. Phys. Lipids* **218**, 91–102. (doi:10.1016/j.chemphyslip.2018.12.006)

28. Haider A *et al.* 2018 PCYT1A Regulates Phosphatidylcholine Homeostasis from the Inner Nuclear Membrane in Response to Membrane Stored Curvature Elastic Stress. *Dev. Cell* **45**, 481-495.e8. (doi:10.1016/j.devcel.2018.04.012)

29. Ces O, Mulet X. 2006 Physical coupling between lipids and proteins: a paradigm for cellular control. *Signal Transduct.* **6**, 112–132. (doi:10.1002/sita.200500079)

30. Marsh D. 1996 Components of the lateral pressure in lipid bilayers deduced from H II phase dimensions. *Biochim. Biophys. Acta* **1279**, 119–123.

31. Beard J, Attard GS, Cheetham MJ. 2008 Integrative feedback and robustness in a lipid biosynthetic network. *J. R. Soc. Interface* **5**, 533–543. (doi:10.1098/rsif.2007.1155)

32. Hague C V., Postle AD, Attard GS, Dymond MK. 2013 Cell cycle dependent changes in membrane stored curvature elastic energy: evidence from lipidomic studies. *Faraday Discuss.* **161**, 481–497. (doi:10.1039/c2fd20078c)

33. Dymond MK. 2016 Mammalian phospholipid homeostasis : evidence that membrane curvature elastic stress drives homeoviscous adaptation in vivo. *J. R. Soc. Interface* , 20160228.

34. Dymond MK. 2015 Mammalian phospholipid homeostasis: Homeoviscous adaptation deconstructed by lipidomic data driven modelling. *Chem. Phys. Lipids* **191**, 136–146. (doi:10.1016/j.chemphyslip.2015.09.003)

35. Alley SH, Ces O, Templer RH, Barahona M. 2008 Biophysical regulation of lipid biosynthesis in the plasma membrane. *Biophys. J.* **94**, 2938–2954. (doi:10.1529/biophysj.107.118380)

36. Dymond MK, Attard GS. 2008 Cationic type I amphiphiles as modulators of membrane curvature elastic stress in vivo. *Langmuir* **24**, 11743–11751. (doi:10.1021/la8017612)

37. Dymond MK, Attard GS, Postle AD. 2008 Testing the hypothesis that amphiphilic antineoplastic lipid analogues act through reduction of membrane curvature elastic stress. *J. R. Soc. Interface* **5**, 1371–1386.

38. Bahja J, Dymond MK. 2021 Does membrane curvature elastic energy play a role in mediating oxidative stress in lipid membranes? *Free Radic. Biol. Med.* **171**, 191–202. (doi:10.1016/j.freeradbiomed.2021.05.021)

39. Corsi J, Dymond MK, Ces O, Muck J, Zink D, Attard GS. 2008 DNA that is dispersed in the liquid crystalline phases of phospholipids is actively transcribed. *Chem. Commun. (Camb).* , 2307–9. (doi:10.1039/b801199k)

40. Wilson RJ, Tyas SR, Black CF, Dymond MK, Attard GS. 2010 Partitioning of ssRNA Molecules between Preformed Monolithic H(II) Liquid Crystalline Phases of Lipids and Supernatant Isotropic Phases. *Biomacromolecules* , 3022–3027. (doi:10.1021/bm1008469)

41. Black CF, Wilson RJ, Nylander T, Dymond MK, Attard GS. 2010 Linear dsDNA partitions spontaneously into the inverse hexagonal lyotropic liquid crystalline phases of phospholipids. *J. Am. Chem. Soc.* **132**, 9728–32. (doi:10.1021/ja101550c)

42. Ma B, Zhang S, Jiang H, Zhao B, Lv H. 2007 Lipoplex morphologies and their influences on transfection efficiency in gene delivery. *J. Control. Release* **123**, 184–94. (doi:10.1016/j.jconrel.2007.08.022)

43. Thurmond RL, Lindblom G, Brown MF. 1991 Effect of bile salts on monolayer curvature of a phosphatidylethanolamine/water model membrane system. *Biophys. J.* **60**, 728–732. (doi:10.1016/S0006-3495(91)82103-8)

44. Simunovic M, Lee KYC, Bassereau P. 2015 Celebrating Soft Matter's 10th anniversary: screening of the calcium-induced spontaneous curvature of lipid membranes. *Soft Matter* **11**, 5030–5036. (doi:10.1039/C5SM00104H)

45. Lewis RNAH, Mannock DA, McElhaney RN, Turner DC, Gruner SM. 1989 Effect of Fatty Acyl Chain Length and Structure on the Lamellar Gel to Liquid-Crystalline and Lamellar to Reversed Hexagonal Phase Transitions of Aqueous Phosphatidylethanolamine Dispersions. *Biochemistry* **28**, 541–548. (doi:10.1021/bi00428a020)

46. Marsh D. 2011 Pivotal surfaces in inverse hexagonal and cubic phases of phospholipids and glycolipids. *Chem. Phys. Lipids* **164**, 177–183. (doi:10.1016/j.chemphyslip.2010.12.010)

47. Armen RS, Uitto OD, Feller SE. 1998 Phospholipid component volumes: determination and application to bilayer structure calculations. *Biophys. J.* **75**, 734–44. (doi:10.1016/S0006-3495(98)77563-0)

48. Fuller N, Benatti CR, Rand RP. 2003 Curvature and bending constants for phosphatidylserine-containing membranes. *Biophys. J.* **85**, 1667–1774.

49. Harper PE, Mannock DA, Lewis RNAH a H, McElhaney RN, Gruner a M, Gruner SM. 2001 X-ray diffraction structures of some phosphatidylethanolamine lamellar and inverted hexagonal phases. *Biophys. J.* **81**, 2693–2706. (doi:10.1016/S0006-3495(01)75912-7)

50. Teague WE, Soubias O, Petrache H, Fuller N, Hines KG, Rand RP, Gawrisch K. 2012 Elastic properties of polyunsaturated phosphatidylethanolamines influence rhodopsin function. *Faraday Discuss.* **161**, 383–395. (doi:10.1039/c2fd20095c)

51. Chen Y-F, Tsang K-Y, Chang W-F, Fan Z -a. 2015 Differential dependencies on [Ca^{2+}] and temperature of the monolayer spontaneous curvatures of DOPE, DOPA and cardiolipin: effects of modulating the strength of the inter-headgroup repulsion. *Soft Matter* **11**, 4041–4053. (doi:10.1039/C5SM00577A)

52. Tate MW, Gruner SM. 1989 Temperature dependence of the structural dimensions of the inverted hexagonal (HII) phase of phosphatidylethanolamine-containing membranes. *Biochemistry* **28**, 4245–4253.

53. Kozlov MM, Leikin S, Rand RP. 1994 Bending, hydration and interstitial energies quantitatively account for the hexagonal-lamellar-hexagonal reentrant phase transition in dioleoylphosphatidylethanolamine. *Biophys. J.* **67**, 1603. (doi:10.1016/S0006-3495(94)80633-2)

54. Peiró-Salvador T, Ces O, Templer RH, Seddon AM. 2009 Buffers may adversely affect model lipid membranes: A cautionary tale. *Biochemistry* **48**, 11149–11151. (doi:10.1021/bi901662b)

55. Siegel DP, Kozlov MM. 2004 The Gaussian curvature elastic modulus of N-monomethylated dioleoylphosphatidylethanolamine: Relevance to membrane fusion and lipid phase behavior. *Biophys. J.* **87**, 366–374. (doi:10.1529/biophysj.104.040782)

56. Kaltenegger M, Kremser J, Frewein MP, Ziherl P, Bonthuis DJ, Pabst G. 2021 Intrinsic Lipid Curvatures of Mammalian Plasma Membrane Outer Leaflet Lipids and Ceramides. *bioRxiv* , 2021.04.26.441390.

57. Gruner SM, Parsegian VA, Rand RP. 1986 Directly measured deformation energy of phospholipid HII hexagonal phases. *Faraday Discuss. Chem. Soc.* **81**, 29–37. (doi:10.1039/DC9868100029)

58. Chen Z, Rand RP. 1997 The influence of cholesterol on phospholipid membrane curvature and bending elasticity. *Biophys. J.* **73**, 267–276. (doi:10.1016/S0006-3495(97)78067-6)

59. Kooijman EE, Chupin V, Fuller NL, Kozlov MM, De Kruijff B, Burger KNJ, Rand PR. 2005 Spontaneous curvature of phosphatidic acid and lysophosphatidic acid. *Biochemistry* **44**, 2097–2102. (doi:10.1021/bi0478502)

60. Kamal MM, Mills D, Grzybek M, Howard J. 2009 Measurement of the membrane curvature preference of phospholipids reveals only weak coupling between lipid shape and leaflet curvature. *Proc. Natl. Acad. Sci. U. S. A.* **106**, 22245–50. (doi:10.1073/pnas.0907354106)

61. Epand RM, Epand RF, Decicco A, Schwarz D. 2000 Curvature properties of novel forms of phosphatidylcholine with branched acyl chains. *Eur. J. Biochem.* **267**, 2909–2915. (doi:10.1046/j.1432-1327.2000.01304.x)

62. Marsh D. 2007 Lateral pressure profile, spontaneous curvature frustration, and the incorporation and conformation of proteins in membranes. *Biophys. J.* **93**, 3884–3899.

(doi:10.1529/biophysj.107.107938)

63. H.N.W. Lekkerkerker. 1989 Contribution Of The Electric Double Layer To The Curvature Elasticity Of Charged Amphiphilic Monolayers. *Physica A* **159**, 319–328.

64. Mulet X, Templer RH, Woscholski R, Ces O. 2008 Evidence that phosphatidylinositol promotes curved membrane interfaces. *Langmuir* **24**, 8443–7. (doi:10.1021/la801114n)

65. Harper PE, Cavazos AT, Kinnun JJ, Petrache HI, Wassall SR. 2020 Vitamin E Promotes the Inverse Hexagonal Phase via a Novel Mechanism: Implications for Antioxidant Role. *Langmuir* **36**, 4908–4916. (doi:10.1021/acs.langmuir.0c00176)

66. Wikström M, Xie J, Bogdanov M, Mileykovskaya E, Heacock P, Wieslander Å, Dowhan W. 2004 Monoglucosyldiacylglycerol, a Foreign Lipid, Can Substitute for Phosphatidylethanolamine in Essential Membrane-associated Functions in Escherichia coli. *J. Biol. Chem.* **279**, 10484–10493. (doi:10.1074/jbc.M310183200)

67. Fuller N, Rand RP. 2001 The influence of lysolipids on the spontaneous curvature and bending elasticity of phospholipid membranes. *Biophys. J.* **81**, 243–254. (doi:10.1016/S0006-3495(01)75695-0)

68. Szule JA, Fuller NL, Rand RP. 2002 The effects of acyl chain length and saturation of diacylglycerols and phosphatidylcholines on membrane monolayer curvature. *Biophys. J.* **83**, 977–984.

69. Leikin S, Kozlov M, Fuller N, Rand R. 1996 Measured effects of diacylglycerol on structural and elastic properties of phospholipid membranes. *Biophys. J.* **71**, 2623–2632.

70. Gillams RJ, Nylander T, Plivelic TS, Dymond MK, Attard GS. 2014 Formation of inverse topology lyotropic phases in dioleoylphosphatidylcholine/oleic Acid and dioleoylphosphatidylethanolamine/oleic Acid binary mixtures. *Langmuir* **30**, 3337–44. (doi:10.1021/la404275u)

71. Burrell J, Dymond MK, Gillams RJ, Parker DJ, Langley GJ, Labrador A, Nylander T, Attard GS. 2017 Using Curvature Power to Map the Domain of Inverse Micellar Cubic Phases: The Case of Aliphatic Aldehydes in 1,2-Dioleoyl-sn-glycero-3-phosphoethanolamine. *Langmuir* **33**, 12804–12813. (doi:10.1021/acs.langmuir.7b02998)

72. Bradford A, Atkinson J, Fuller N, Rand RP. 2003 The effect of vitamin E on the structure of membrane lipid assemblies. *J. Lipid Res.* **44**, 1940–5. (doi:10.1194/jlr.M300146-JLR200)

73. Lähdesmäki K, Ollila OHS, Koivuniemi A, Kovanen PT, Hyvönen MT. 2010 Membrane simulations mimicking acidic pH reveal increased thickness and negative curvature in a bilayer consisting of lysophosphatidylcholines and free fatty acids. *Biochim. Biophys. Acta - Biomembr.* **1798**, 938–946. (doi:10.1016/j.bbamem.2010.01.020)

74. Hunter JE, Brandsma J, Dymond MK, Koster G, Mark Moore C, Postle AD, Mills RA, Attard GS. 2018 Lipidomics of Thalassiosira pseudonana under phosphorus stress reveal underlying phospholipid substitution dynamics and novel diglycosylceramide substitutes. *Appl. Environ. Microbiol.* **84**, 1–17. (doi:10.1128/AEM.02034-17)

75. Caforio A, Driessen AJM. 2017 Archaeal phospholipids: Structural properties and biosynthesis. *Biochim. Biophys. Acta - Mol. Cell Biol. Lipids* **1862**, 1325–1339. (doi:10.1016/j.bbalip.2016.12.006)

76. Brooks NJ, Ces O, Templer RH, Seddon JM. 2011 Pressure effects on lipid membrane structure and dynamics. *Chem. Phys. Lipids* **164**, 89–98. (doi:10.1016/j.chemphyslip.2010.12.002)

Accepted version: Chemistry and Physics of Lipids 239C (2021) 105117
Received 24 April 2021, Revised 3 July 2021, Accepted 9 July 2021, Available online 12 July 2021.